American Mineralogist, Volume 72, pages 801–811, 1987

Cathodoluminescence and microprobe study of rare-earth elements in apatite

PETER L. ROEDER, DUNCAN MACARTHUR, XIN-PEI MA, GERALD R. PALMER
Queen's University, Kingston, Ontario K7L 3N6, Canada
ANTHONY N. MARIANO
48 Page Brook Road, Carlisle, Massachusetts 01741, U.S.A.

ABSTRACT

The cathodoluminescence (CL) spectrum was scanned from 400 to 700 nm for each of fourteen apatite crystals from carbonatites, pegmatites, nelsonites, and granites. Peaks due to activation by Sm^{3+}, Dy^{3+}, Tb^{3+}, Eu^{3+}, Eu^{2+}, and Mn^{2+} were identified in the CL spectra. Proton (PIXE) and electron-microprobe analyses were used to determine the major (Ca, P, F) and minor elements (As, Si, Th, Mn, Fe, Sr, Na, Cl, REEs) in the apatite crystals. The microprobe analysis of two of the apatite samples (Durango and Huddersfield) compare favorably with analyses reported in the literature for apatite samples from the same localities. The rare-earth-element (REE) content varies from 0.2 to more than 15 wt% and is generally proportional to Na + Si, suggesting charge compensation for substitution of REE^{3+} for Ca^{2+}. The chondrite-normalized distribution of the REEs shows light REE enrichment for the majority of samples with the Ce/Y ratio varying from 30 to 0.1. The relative height of the Sm^{3+} and Dy^{3+} peaks in the CL spectrum was found to be a good guide to the relative light to heavy REE enrichment. Apatites from more alkaline environments tended to be richest in the light REEs. The CL spectrum for an apatite from the Llallagua tin deposit in Bolivia shows a broad Eu^{2+} peak at a short wavelength and narrow Eu^{3+} peaks superimposed on a broad Mn^{2+} peak at a longer wavelength. The peak assignment was confirmed using an ultraviolet source and by comparison with spectra from synthetic apatite. The chondrite-normalized REE distribution for this sample shows a large positive Eu anomaly, which is similar to the positive anomaly shown for an apatite from the Panasqueira tin deposit in Portugal.

A series of glasses doped with Eu and heated at 1400°C at a series of oxygen fugacities was used to show the effect of oxygen fugacity on the relative height of the Eu^{2+} and Eu^{3+} peaks in the CL spectrum. It is concluded from these spectra that the positive Eu anomaly in the apatite from Llallagua and Panasqueira was not due to the preferential incorporation of Eu^{2+} by the apatite structure, but rather to the crystallization of the apatite from a reservoir strongly enriched in Eu.

INTRODUCTION

Apatite is one of the most common accessory minerals found in crustal rocks, and its presence and distribution are often used to model geologic processes such as mantle melting, differentiation in magma chambers, and hydrothermal processes (e.g., Nash, 1972; Henderson, 1980; Kovalenko et al., 1982). The structure of apatite is such that it concentrates many elements that are found only in trace amounts in the Earth's crust, in particular the rare-earth elements (REEs). Apatite and the REEs are often concentrated in carbonatites and associated alkaline rocks that are important as ore deposits of phosphates, REEs, Nb, Y, U, etc. One very important tool in the exploration of carbonatites is cathodoluminescence (Mariano, 1978), which can be used to estimate the distribution and kind of REE present in many minerals. The present study involved the chemical analysis of the apatite for REEs using the electron and proton microprobes and the correlation of the REE distribution to the cathodoluminescent spectra of the apatite.

Naturally occurring apatites can be represented by the formula $Ca_{10}(PO_4)_6F_2$, with many substitutions possible for Ca, P, and F. Minor replacement of Ca in natural apatites is mainly by Na, Sr, Mn, and the REE. The most common substitution for P is by Si, coupled with a substitution of Ca by trivalent REE ions. Smaller amounts of As, S, V, and also carbonate ion are possible. F is replaced mainly by Cl and $(OH)^-$. The fact that virtually all apatite shows cathodoluminescence indicates that very limited amounts of Fe^{2+} substitutes for Ca in the structure, because Fe^{2+} is an effective quencher for cathodoluminescence (CL) in most minerals.

The REEs have become very important in geochemical modeling. They act as a cohesive group of elements with very similar chemical characteristics (Henderson, 1984), but there are subtle chemical differences between the light

0003–004X/87/0708–0801$02.00

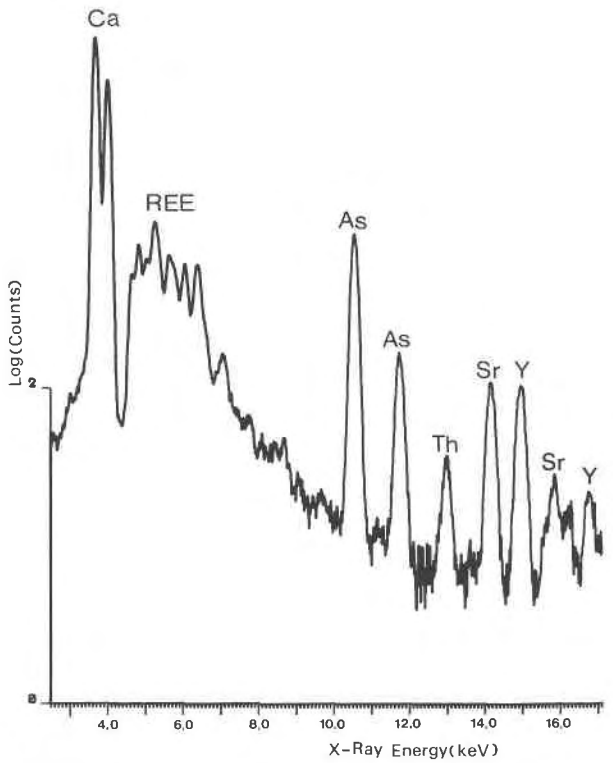

Fig. 1. Proton-induced X-ray spectrum of the Durango apatite.

rare-earth elements (LREEs) and the heavy rare-earth elements (HREEs). The LREE ions in oxygen-dominated structures tend to be larger than the HREE ions, and the electronic configuration sometimes favors the 4+ state of Ce and the 2+ state for Eu. Apatite has often been used as an example of a mineral that tends to concentrate the LREEs or the middle rare-earth elements relative to the HREEs, but the actual REE distribution in a particular apatite depends not only on the apatite structure, but upon the REE distribution and chemical characteristics of the melt, rock, or fluid reservoir from which the apatite crystallized (Papike et al., 1984). Thus Watson and Green (1981) have shown that apatite crystallizing from a granitic melt has a fourfold increase in its ability to concentrate REEs compared to apatite crystallizing from a basaltic melt. The oxidation state of the reservoir is also very important since elements such as Ce (Ce^{3+}, Ce^{4+}) and Eu (Eu^{2+}, Eu^{3+}) are sensitive to the oxygen fugacity of the reservoir. The distribution of the REEs in apatite crystallizing from residual melts or hydrothermal solutions may be sensitive to the stability of REE molecular complexes in the solutions or melts (Flynn and Burnham, 1978; Taylor and Fryer, 1982). Subtle changes in acidity and alkalinity of the solution may be reflected in the REE distribution of the crystallizing apatite, and apatite forming at different stages may have a different REE concentration and distribution (Shmakin and Shiryayeva, 1968). The complicated zoning in some apatite crystals (Knutson et al., 1985) reflects changing chemical conditions during growth. The zoning of REEs may be preserved because of the very low diffusion rate of REEs in the apatite structure (Watson et al., 1985). Thus the ubiquitous presence of small amounts of apatite may be used to record chemical and physical changes in the environment of crystallization and to correlate stages of growth. In order to use the REE distribution in apatite to its full potential, it is best to analyze this distribution using a nondestructive technique with a high spatial resolution, a microprobe (ion, electron, or proton) or an optical technique such as ultraviolet- or electron-excited luminescence.

The electron microprobe is the most convenient type of microprobe to analyze the major elements in apatite. It combines a high spatial analyzing resoltuion of better than 5 μm, a very stable electron flux, and a very good peak resolution using a wavelength-dispersive spectrometer. The high bremsstrahlung background produced by the electron flux makes it difficult to analyze REEs at levels much lower than a few hundred ppm (Roeder, 1985). The proton microprobe (PIXE) can, with suitable apertures and focusing magnets, produce a high-energy source of protons with a useful resolution of a few micrometers and a spectrum with a much lower background level than that from the electron microprobe. Thus the REEs can, in principle, be measured at levels of a few ppm; and, in practice, levels of a few tens of ppm are achievable. A proton-induced X-ray emission (PIXE) spectrum of a Durango apatite using an energy-dispersive spectrometer is shown in Figure 1. The proton- and electron-microprobe analysis for this sample (Probe) is compared in Table 2 to two published analyses.

Virtually all naturally occurring apatites show luminescence in the visible spectrum when exposed to ultraviolet, laser, or electron excitation. The luminescence is due to impurity elements that function as activators or coactivators in the apatite host. A pure apatite crystal without activator impurities or vacancies exhibits no luminescence. The principal activators in natural apatites are Mn^{2+}, Sm^{3+}, Dy^{3+}, Tb^{3+}, Eu^{2+} and Eu^{3+} (Mariano and Ring, 1975). The luminescence response of these activators is so efficient that crystals as small as 20 μm are vividly revealed, even for activator concentrations well below 100 ppm. This characteristic of apatite is an asset to the petrographer because even though apatite is one of the most ubiquitous accessory minerals in rocks, it frequently occurs as small crystals whose recognition is often obscured due to association with other minerals.

Synthetic apatite is the main host material for phosphors used in fluorescent lights, and rare-earth–activated fluorapatite has been synthesized for solid-state laser crystals. Emission spectra for most of the activators in apatite are well documented in the literature (e.g., Mariano, 1978), and interpretation of CL emission spectra in apatite has been made by correlation with work on synthetic apatites. The principal activator in natural apatites is Mn^{2+}, which produces a broad band in the yellow-

green part of the visible spectrum. The wavelength of emission is not only determined by an electron transition of the free ion but by the crystal-field influence of the host, so that variations in the emission wavelength often occur. The trivalent REE activators each show several narrow bands whose wavelength of emission is only slightly affected by the crystal field of the host. The wavelength of emission from Eu^{2+}, however, is sensitive to structural changes within a host crystal because the transitions for this ion involve poorly shielded valence electrons (Palilla and O'Reilly, 1968). The peak positions and relative intensities of the emissions for various REEs are very complex and will be discussed in greater detail in a later section. Eu and, to a much lesser extent, Sm are naturally occurring REEs that commonly occur in both the 3+ and 2+ state and show emission peaks for both oxidation states. These peaks for Eu occur both in the red and blue part of the spectrum, and thus the use of ultraviolet and cathodoluminescence can be a guide to the oxidation state of Eu. Emission spectra (CL and UV) for apatite from various geologic environments has been studied by many workers including Portnov and Gorobets (1969), Ovcharenko and Urev (1971), Mariano and Ring (1975), Mariano (1978), and Huaxin (1980). The identification of the activators and their relative abundance in apatites serve as petrogenetic indicators, and there have been many attempts to use the cathodoluminescence for this purpose. The use of CL has been mainly as a qualitative tool because apatites found in nature are chemically too complex to determine the relative effects of activator, coactivator, and quenching elements on the emission spectra. However, it is the fairly dramatic change in the visible spectra produced by subtle changes in the trace elements that make cathodoluminescence useful to discriminate different stages of crystal growth.

Experimental techniques

The electron-microprobe analyses were done at Queen's University using an ARL-SEMQ microprobe at 15 and 25 kV. The Ca and P analyses were carried out using energy-dispersive analysis with a Si detector (155 eV FWHM resolution at Mn$K\alpha$) and synthetic $Ca_2P_2O_7$ as a standard. The other elements (F, Na, Si, Cl, REEs) were analyzed by wavelength-dispersive analysis using methods similar to those described by Roeder (1985).

The PIXE spectrum presented in Figure 1 was obtained with an external beam of 3.0-MeV protons from the Queen's University Van de Graaff accelerator. The specimens, mounted in epoxy and polished, were all larger than 100 μm in size so that a final aperture of 25 μm was used. With a beam energy of 3 MeV and a current of a few nanoamperes, spectra with sufficient statistical accuracy for analysis were obtained in ~1000 s. Pile-up of Ca and P signals, which would interfere with the REE spectra between 6 and 8 keV was reduced to an insignificant amount (0.2%) with a 86 mg/cm^2 (650 μm) mylar absorber, which also reduced the transmission of the La L X-rays to 5%. This was not a serious problem since the LREEs are normally the dominant ones.

The proton probe used an energy-dispersive system with a resolution of 160 eV FWHM (Mn$K\alpha$), and the quantity of each REE (plus Fe and Mn) was determined with a spectrum-stripping procedure (Ma et al., 1987) utilizing an accurately determined response function for a single element in a matrix similar to that of the actual specimens. These functions were obtained as mathematical expressions from experimentally measured spectra of a single REE in a phosphate crystal. The expressions consisted of a number of Gaussian peaks positioned at the expected energies of the strong L X-rays, with the ratio of the peaks adjusted slightly from the values given by Mitchell and Ziegler (1977) to match the observed spectra. Eleven L X-ray lines were needed to accurately reproduce a spectrum.

TABLE 1. REEs (wt%) in glass S-253

	Nom	EMP	PIXE	Neutron activation analyses		
				1	2	3
La	0.08	0.06	0.073	0.075	0.090	0.100
Ce	0.08	0.06	0.072	0.070	0.079	0.100
Pr	0.08	0.08	0.076			
Nd	0.08	0.08	0.076		0.067	0.100
Sm	0.08	0.06	0.068	0.075	0.087	0.097
Eu	0.08	0.08	0.070	0.074	0.077	0.088
Gd	0.08	0.08	0.071		0.095	
Tb	0.08	0.07	0.077	0.078	0.080	0.088
Dy	0.08	0.06	0.095		0.080	
Ho	0.08	0.07	0.075		0.097	
Er	0.08	0.06	0.080			
Tm	0.08	0.05	0.076		0.077	
Yb	0.08	0.06	0.076	0.074	0.080	0.088
Lu	0.08	0.06	0.070	0.075	0.080	0.086

Note: Columns are as follows: Nom = nominal wt% from initial weighing (Roeder, 1985); EMP = electron-microprobe analysis; PIXE = external beam proton microprobe, Queen's University; 1 = analysis by N. Eby, University of Lowell, Lowell, Massachusetts, U.S.A. (interlaboratory standard was "BASALT"); 2 = analysis of GINA (Université de Montréal, Montreal, Quebec); 3 = analysis by Neutron Activation Services, McMaster Nuclear Reactor, Hamilton, Ontario.

The PIXE spectra were calibrated with a glass standard (S-254) containing 1% of each REE as described by Roeder (1985). The spectra from this standard were analyzed in exactly the same way as those from the specimens. Thus the ratio of the counts for an element in a sample to the counts in the standard gave the concentration of the element directly. For those analyses on small samples where some doubt existed as to whether the total proton beam hit the target, the Ca concentration determined with the proton microprobe was made equal to that determined with the electron microprobe, thus effectively normalizing the concentrations for the REEs.

The reproductibility of the analyses of the Durango apatite was determined to be better than 10% for reasonably strong lines, e.g., La, Ce, Nd, and well-resolved lines such as As and Sr, decreasing to 25% for elements such as Pr, Gd, and Dy. The results of the analyses on the various apatites are given in Table 2. Since several samples of the same apatite were usually available, the analyses are usually the average of two or three measurements on the different samples.

A glass (S-253, available from Roeder) containing a nominal 0.08 wt% of each REE (Roeder, 1985) was analyzed for REEs by electron (EMP) and proton (PIXE) microprobes. These analyses are shown in Table 1 together with three neutron-activation analyses of this glass. Although there is considerable variation of the REEs, the average PIXE analysis is close to the nominal 0.08 wt%.

A glass having the approximate composition CaO = 9, MgO = 22, Al_2O_3 = 16, SiO_2 = 52% was doped with 1% europium oxide in order to determine the effect of oxygen fugacity on the CL spectrum of Eu. Each glass sample was heated at 1400°C for 24

TABLE 2. Analyses (wt%) of apatite

	1—Durango			2—Huddersfield			3—Australia	4—Blue River		5—Snarum	
	Microprobe	Young et al., 1969	Rogers et al., 1984	Microprobe	Cruft et al., 1965	Trzcienski et al., 1974	Microprobe	Microprobe	NAA	Microprobe	NAA
P_2O_5	40.90	40.78		38.32	38.37	38.26	35.25	41.77		41.98	
As_2O_5	0.133	0.09		0.008			<0.001	<0.001		0.001	
SiO_2	0.04			1.07	1.07	1.76	0.05	0.060		0.06	
ThO_2	0.024			0.083			0.004	0.001		0.004	
CaO	54.05	54.02		53.44	53.98	53.91	50.42	54.14		51.56	
MnO	0.011	0.01		0.015	0.01		0.003	0.035		0.010	
FeO	0.028	0.05		0.034	0.04	0.12	0.031	0.112		0.084	
SrO	0.059	0.07		0.207	0.27	0.28	0.051	0.429		0.028	
Na_2O	0.10	0.23		0.04		0.28	1.04	0.12		0.30	
F	3.53	3.53		3.97	3.30	3.92	3.44	2.53		0.71	
Cl	0.36	0.41		n.d.	0.20		0.01	0.01		4.79	
Y_2O_3	0.072	0.097		0.114	0.18	0.15	0.275	0.014		0.395	
La_2O_3	0.414	0.493	0.416	0.328	0.35	0.44	0.001	0.094	0.107	0.098	0.094
Ce_2O_3	0.505	0.551	0.517	0.811	0.96	1.23	0.021	0.193	0.232	0.298	0.281
Pr_2O_3	0.069	0.094	0.050	0.094			0.015	0.018		0.062	
Nd_2O_3	0.151	0.233	0.150	0.405			0.007	0.079	0.112	0.255	0.244
Sm_2O_3	0.019	0.035	<0.006	0.040			0.014	0.021	0.020	0.079	0.087
Eu_2O_3	0.006	0.002	0.012	0.012		0.001	0.001	0.003	0.010	0.010	0.011
Gd_2O_3	0.045	0.023	0.030	0.078			0.042	0.014		0.094	
Tb_2O_3	0.027	0.012	0.044	0.033			0.004	0.001	0.002	0.029	0.020
Dy_2O_3	0.021	0.017	0.026	0.029			0.026	0.007		0.075	
Ho_2O_3	<0.005	0.003	0.005	<0.005			0.008	<0.009		0.034	
Er_2O_3	<0.005	0.011	<0.002	<0.005			0.029	<0.006		0.055	
Tm_2O_3	<0.004	0.001	0.005	<0.004			0.006	<0.006		0.016	
Yb_2O_3	0.006	0.006	0.011	0.008			0.031	<0.005	0.001	0.054	0.031
Lu_2O_3	0.004	0.001		0.003			0.001	<0.004		0.010	
Total*	99.01			97.47			89.33	98.58		99.71	
				Ions per 26 O + F + Cl							
Ca site	10.066			10.223			10.800	10.101		9.753	
P site	5.959			5.883			5.733	6.088		6.141	
F + Cl	2.019			2.203			2.089	1.378		1.787	
Na + Si	0.040			0.201			0.396	0.050		0.110	
Y + REEs	0.085			0.127			0.041	0.028		0.106	

Note: Sample numbers correspond to those given in the text. Microprobe analyses were conducted using the electron and proton microprobes. The neutron-activation analyses (NAA) were conducted by Nelson Eby, University of Lowell, Lowell, Massachusetts, U.S.A.

* Total is corrected for oxygen equivalent of fluorine.

h in air or at an oxgen fugacity controlled by mixing CO_2 and H_2 (Jamieson and Roeder, 1984).

The cathodoluminescence (CL) spectra were collected using electron excitation from a Nuclide Luminoscope (R) ELM-2A, which consists of a cold cathode discharge that provided energies variable between 5 and 15 keV and beam currents up to 800 nA. The CL spectra of the luminescing minerals were recorded with a Gamma Scientific model 3000 AR scanning spectroradiometer and a more recent model NM-3 monochromator system, which also includes an SC-1 scanning control; a model D-43 extended-spectral-range (250–930 nm) side-looking photomultiplier detector; and a model DR-1 digital radiometer. The experimental conditions are similar to those described by Mariano and Ring (1975). For the generation of the CL spectra, an electron-beam diameter of approximately 2 mm was employed.

RESULTS

The fourteen apatites that have been studied are described in Appendix 1. The electron microprobe (EMP) and proton microprobe (PIXE) analyses of the apatites are shown in Table 2 in the columns labeled "Probe." The elements P, Si, Ca, Na, F, and Cl were analyzed by EMP, and the other elements were analyzed by PIXE. The one exception is sample 6, which contains a major amount of REEs, and it was thought that the EMP results for La, Ce, Pr, Sm, and Gd were more accurate. The Durango and Huddersfield apatites are well known and have been studied in considerable detail. The microprobe analyses of these two samples are compared in Table 2 with analyses by other workers on different samples from the same localities. The microprobe analysis of the Durango sample compares favorably with the wet-chemical and spectrographic analysis of Young et al. (1969) and with the PIXE analysis of Rogers et al. (1984). The Huddersfield apatite was very carefully analyzed by Cruft et al. (1965), using wet-chemical analysis and was analyzed again by Trzcienski et al. (1974). The microprobe analysis compares favorably with both of these earlier studies, and any differences may be explained by natural heterogeneity. The REEs for a few apatite samples were also analyzed by N. Eby using neutron activation (NAA) and are shown in a separate column. The results of the microprobe and neutron-activation analytical techniques agreed quite well,

TABLE 2. *Continued*

6—Paja-rito	7—Timmins	8—Kerimasi	9—Llallaqua		10—Mt. Pass	11—Tapira		12—Khibina	13—Mineville		14—Oka
Micro-probe	Micro-probe	Micro-probe	Micro-probe	NAA	Micro-probe	Micro-probe	NAA	Micro-probe	Micro-probe	NAA	Micro-probe
36.55	40.84	40.09	42.35		38.62	40.35		39.04	34.89		37.19
0.003	0.003	<0.001	<0.001		0.013	<0.001		<0.001	0.330		0.003
1.71	0.56	0.60	0.14		0.60	0.55		0.24	3.30		1.79
0.010	0.007	0.005	<0.002		0.115	<0.002		0.009	0.258		0.030
38.35	54.43	54.11	54.63		51.13	53.74		51.95	47.93		51.76
0.065	0.044	0.018	0.139		0.037	0.007		0.013	0.051		0.048
0.169	0.549	0.158	0.032		0.077	0.026		0.009	0.347		0.091
0.200	0.175	0.939	0.046		3.019	1.029		3.058	0.057		0.906
2.63	<0.01	0.01	<0.01		0.26	<0.01		0.01	0.02		0.07
3.65	3.99	2.38	3.74		3.52	1.77		3.33	3.20		2.65
0.01	0.02	0.04	0.05		0.16	0.02		0.01	0.04		0.01
0.306	0.337	0.021	0.016		0.090	0.020		0.032	1.888		0.075
4.48	0.096	0.136	0.020	0.006	0.442	0.109	0.118	0.273	1.614	1.208	0.771
8.50	0.130	0.275	0.027	0.010	0.910	0.176	0.159	0.416	3.182	2.691	1.500
0.93	0.007	0.049	0.007		0.111	0.045		0.027	0.366		0.246
3.69	0.084	0.068	0.017		0.429	0.053	0.071	0.143	1.585	1.186	0.503
0.50	0.036	0.016	0.014	0.003	0.080	0.006	0.012	0.028	0.304	0.240	0.058
<0.059	0.002	<0.002	0.146	0.114	0.020	0.003	0.004	0.008	0.037	0.021	0.019
0.33	0.065	0.024	<0.005		0.080	0.018		0.033	0.361		0.089
0.477	0.020	0.014	<0.004	0.001	0.052	0.009	0.001	0.019	0.194	0.049	0.069
<0.033	0.083	0.020	<0.004		<0.013	0.008		<0.006	0.189		0.003
<0.082	0.015	<0.006	0.001		<0.010	<0.003		<0.006	0.062		<0.011
<0.024	0.046	<0.004	<0.004		<0.009	<0.003		<0.005	0.167		<0.009
<0.005	0.028	<0.004	<0.004		0.008	<0.001		<0.005	0.051		<0.008
<0.017	0.044	0.007	0.003	0.001	0.006	0.009	0.001	<0.005	0.174	0.123	<0.007
<0.015	<0.005	<0.001	<0.005		0.005	0.005		0.001	0.059		<0.006
101.11	99.93	97.97	99.79		98.25	97.20		97.25	99.30		96.76
					Ions per 26 O + F + Cl						
9.869	10.053	10.290	9.880		10.267	10.270		10.272	10.089		10.339
6.017	5.954	6.032	6.048		5.897	6.107		5.912	5.968		5.986
2.130	2.144	1.326	2.001		2.019	0.990		1.873	1.841		1.510
1.255	0.094	0.108	0.023		0.195	0.096		0.046	0.603		0.346
1.299	0.068	0.040	0.015		0.144	0.029		0.064	0.720		0.219

and usually when there was a significant difference between techniques, the results for all the elements would be lower or higher (sample 13).

The ionic proportions were calculated for each analysis; however, only a summary of the ionic proportions is shown at the bottom of each analysis in Table 2 (complete ionic proportions are available from P. L. Roeder). The ionic proportions generally fit the formula $Ca_{10}(PO_4)_6F_2$. It has been assumed that As^{5+} and Si^{4+} substitute for P^{5+}, whereas Cl^- substitutes for F^-, and the other cations substitute for Ca^{2+}. It is believed that most of the major species in the apatite have been analyzed, except for carbon dioxide and water. The sample showing the greatest deviation from the proportions 10:6:2 is the Australian sample (3), which gave a very poor analytical total; this may be because the surface of the polished section had many small holes, which may reflect the original crystal growth in the lateritic weathering profile. Thus the texture of this sample may not have been ideal for normal microprobe techniques; however, the low analytical total may also be due to the presence of other species such as carbon dioxide and water. It has been noted by many workers (e.g., Watson and Green, 1981) that most of the REEs may substitute in apatite as trivalent cations with the concomitant substitution of Si^{4+} for P^{5+} to provide a charge balance. We have found that this is generally true; however, we found an even better correlation of the Y + REE substitution with the substitution of Na^{1+} plus Si^{4+}. This can be seen by comparing the Na + Si and Y + REE columns at the bottom of Table 2. Thus the charge-balanced substitution may be shown as follows: $REE^{3+} + Na^+ \rightarrow Ca^{2+} + Ca^{2+}$ and $REE^{3+} + Si^{4+} \rightarrow Ca^{2+} + P^{5+}$. One of the factors that may control whether Na or Si substitutes with the REEs is the degree of silica saturation (or the alkalinity) of the reservoir from which the apatite crystallized.

The total REEs are quite variable between samples, and so also is the distribution of individual REEs. A convenient method of discriminating between the degree of LREE (Ce group) relative to HREE (Y group) enrichment is to use the Ce/Y ratio. The REE distribution relative to the concentration of the REEs in chondritic meteorites is

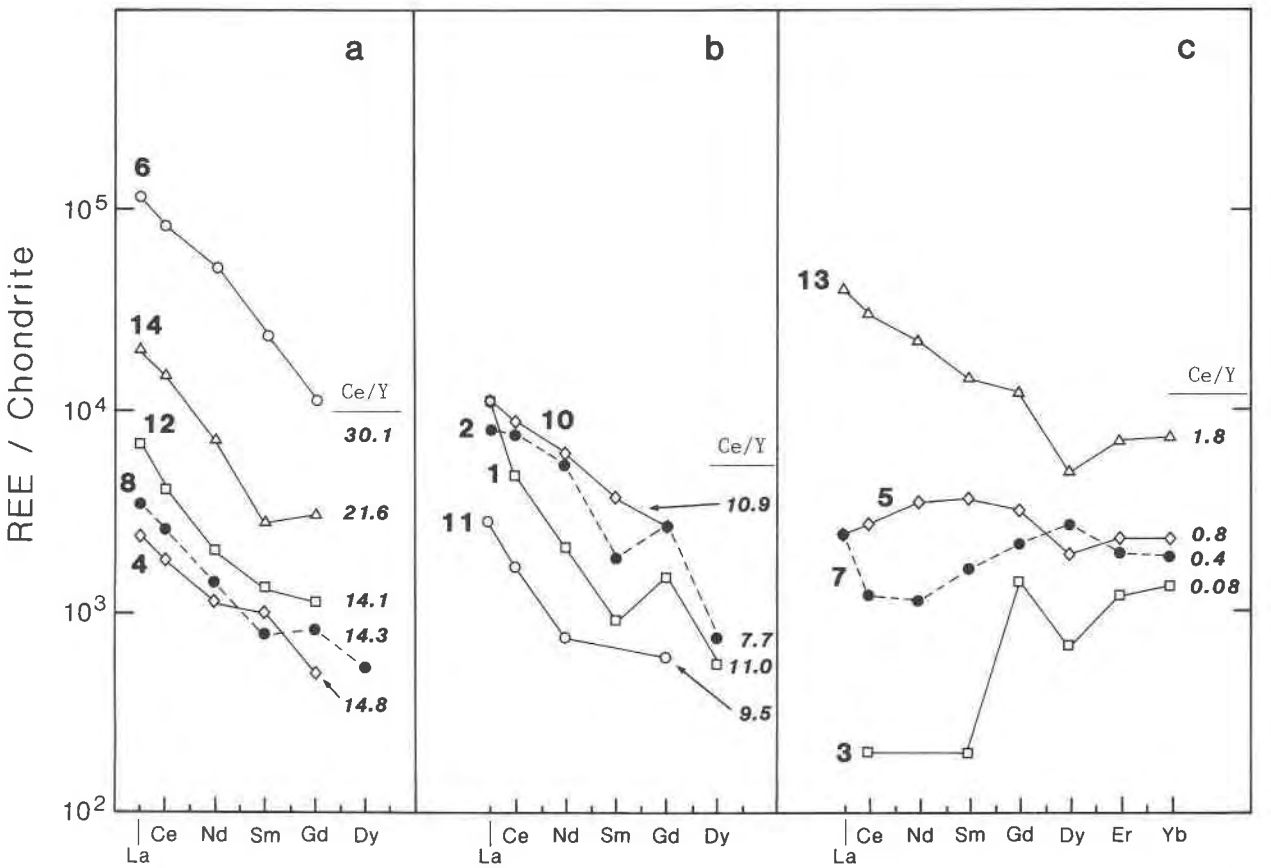

Fig. 2. REEs in apatite normalized to the distribution found in a chondritic meteorite. The sample number is shown in bold type to the left of each curve and the Ce/Y ratio is shown to the right of each curve.

plotted in Figure 2. Only those REEs with values over 100 ppm and only the even atomic-numbered REE (including La) have been plotted, because of the general low levels of odd-numbered REEs and thus the increased analytical uncertainty. Figures 2a, 2b, 2c are shown in the order of degrees of LREE to HREE enrichment. The Llallagua sample (9) has been omitted from Figure 2 because of the low level of most of the REEs and the unique Eu anomaly, which will be discussed in greater detail in a later section.

Many workers (e.g., Amli, 1975) have pointed out the general enrichment of LREEs in apatite. However, some of the apatite samples shown in Figure 2c do not show LREE enrichment, and the partition coefficient data of Watson and Green (1981) suggest that the apatite structure may not concentrate LREEs relative to the HREEs. The LREE enrichment often found in apatite is probably due to the crystallization of apatite from a reservoir with LREE enrichment. Apatites that have grown in alkaline environments, such as carbonatites, have often been cited (e.g., Fleischer and Altschuler, 1982) as showing a strong LREE enrichment. This has been confirmed in the present study. The apatite samples (2, 4, 6, 8, 10, 11, 12, 14) that can be identified as from a very alkaline environment have Ce/Y ratios ranging from 30.1 to 7.7. The Pajarito apatite (6) has a very high total REE content and the highest Ce/Y ratio and still maintains the apatite structure, as determined by X-ray diffraction (R. C. Peterson, pers. comm., 1986). The compilations of Fleischer and Altschuler (1982, 1986) of more than 900 REE analyses in apatite showed that the general provenance of the apatite could be determined by the REE distribution. The present data on the carbonatite apatite are consistent with the observations that apatite from carbonatites are LREE enriched with a low Y/REE ratio and high total REE content.

The visible luminescence spectrum for each of the analyzed apatites was measured using electron excitation (CL), and these spectra are shown in Figure 3. The major peaks have been labeled with the most probable element and oxidation state that produced the peak. The element assignment is consistent with most of the earlier work (e.g., Mariano and Ring, 1975; Langurwey, 1977; Marfunin, 1979) and with the spectra collected in the present study using separate REE phosphates synthesized by L. Boatner. The most prominent peak in apatites showing LREE enrichment (high Ce/Y ratio) is due to Sm^{3+} (λ = 595 nm), whereas the major Dy^{3+} peak (λ = 568 nm) only

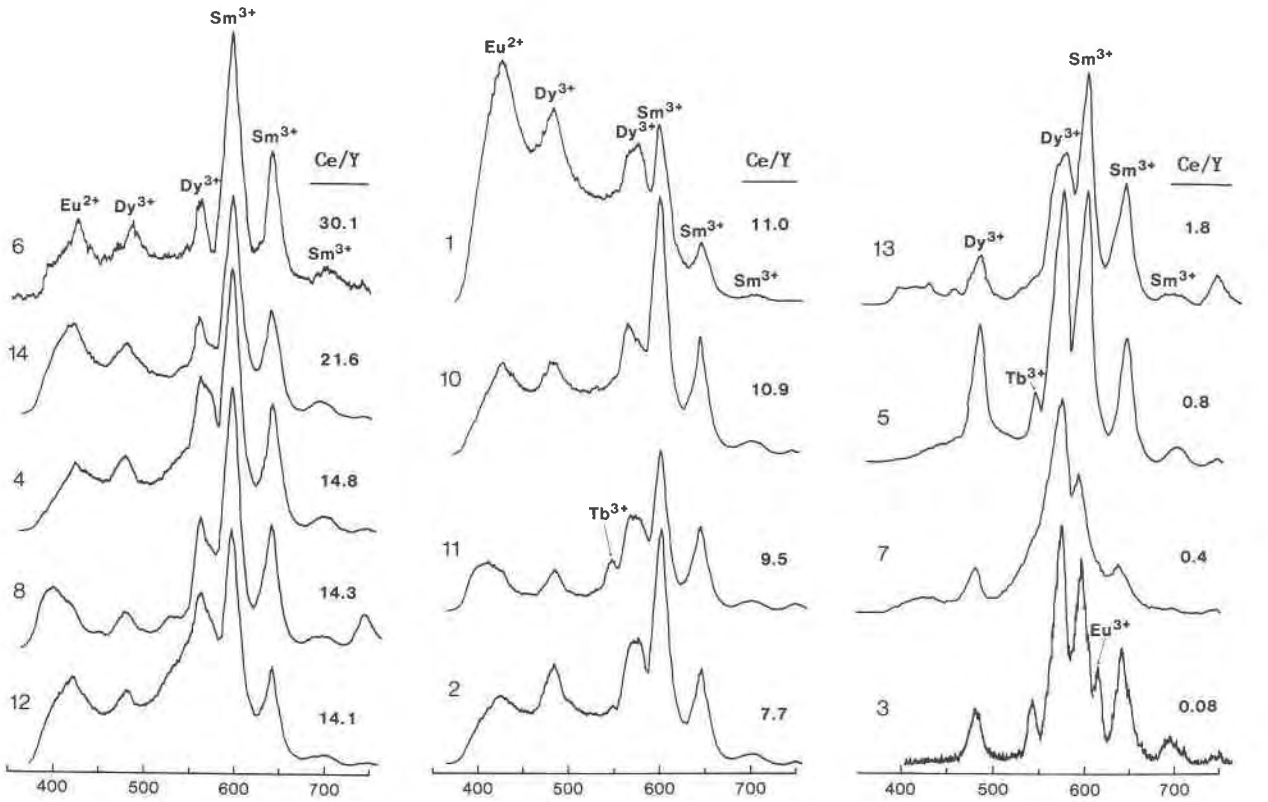

Fig. 3. Cathodoluminescence spectra of apatite with the wavelength plotted from 400 to 700 nm. The sample number is to the left and the Ce/Y ratio to the right of each curve. The most probable element and oxidation state for the peaks are shown.

becomes prominent in apatites with a low Ce/Y ratio or slight LREE enrichment. Thus the relative height of the Sm^{3+} (595 nm) and Dy^{3+} (568 nm) peaks can be used as a guide to the relative degree of LREE enrichment. The major Sm^{3+} (595 nm) and Dy^{3+} (568 nm) peaks sometimes seem to coalesce (sample 7) because a very broad Mn^{2+} peak becomes prominent. The broad Mn^{2+} peak is shown in a Mn-doped synthetic apatite in Figure 4d, and the broad Mn peak (560 nm) dominates the Llallagua apatite in Figure 4a. Sample 3 from a lateritic weathering profile has the lowest Mn content of all the apatites and shows (Fig. 3) excellent resoltuion of the Sm^{3+} and Dy^{3+} peaks due to the absence of the broad Mn^{2+} peak. The Mn^{2+} peak is often absent in samples from oxidizing environments. In these environments, there may be abundant manganese oxides with Mn^{4+}, but there is little Mn^{2+} in the minerals. The spectrum of sample 3 (Fig. 3) also shows a well-resolved peak at 615 nm that is probably due to Eu^{3+}. The absence of a Eu^{2+} peak may reflect the oxidizing conditions during crystallization. The peak at 480 nm has been assigned to Dy^{3+}, but for some samples this may be questionable because the ratio of the height of the Dy^{3+} peak at 568 nm to the other Dy peak is quite variable. Although Tb is usually present in only trace amounts, the major Tb^{3+} peak ($\lambda = 540$ nm) is often found [Tapira (11), Kerimasi (8), Snarum (5), Australian (3)]. Most of the major peaks (Fig. 3) are in the yellow-orange (560–600 nm) part of the spectrum because the dominant activators are Sm^{3+}, Dy^{3+}, and Mn^{2+}. The Durango (1) spectrum has a strong blue component because of a peak that is tentatively identified as Eu^{2+}. Many of the spectra show a peak in the 400–450-nm range, which has been shown at the position of Eu^{2+} but is likely due to some other unknown activator (e.g., Ce^{3+} or a crystal-defect mechanism).

The spectra for the Llallagua (9) apatite are shown in Figures 4a and 4b together with other samples showing prominent Mn^{2+} and Eu peaks. The Llallagua CL spectrum (Fig. 4a) is dominated by the broad Mn^{2+} peak on which are superimposed four Eu^{3+} peaks (585, 613, 645, 690 nm). These Eu^{3+} peaks show up much better using a UV source (Fig. 4b) because the UV is less efficient at generating the broad Mn^{2+} peak. The peak at 450 nm is identified as due to Eu^{2+}. This peak is better seen in Figure 4c, which is from a synthetic apatite doped with Eu, and thought to have been synthesized at the low oxygen fugacity produced by H_2 gas. Silicate glasses doped with 1% Eu were prepared at different oxygen fugacities at 1400°C in order to confirm the assignment of Eu^{2+} and Eu^{3+} lines and to show the relative peak heights as a function of oxygen fugacity. Figure 5 shows the CL spectra of these glasses together with the logarithm of the oxygen fugacity. The glass prepared in air ($\log f_{O_2} = -0.7$) was run at an oxygen fugacity higher than that expected

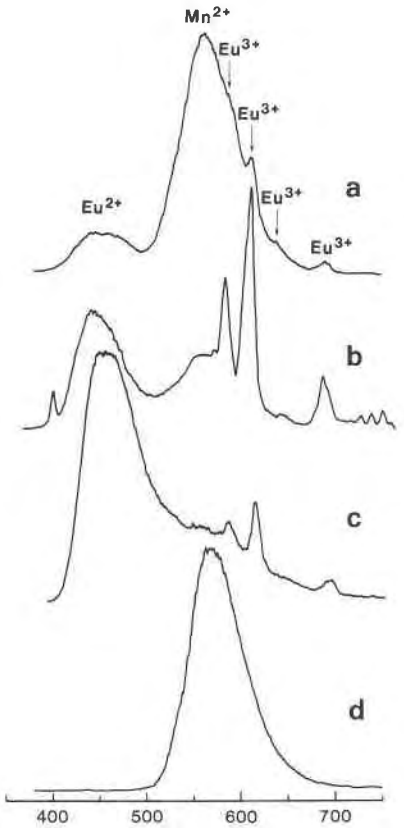

Fig. 4. (a) Cathodoluminescence and (b) ultraviolet-induced spectra for the Llallagua apatite (sample 9) plotted from 400 to 700 nm. Spectrum (c) is of an apatite doped with Eu and synthesized at low oxygen fugacity. Spectrum (d) is of a synthetic apatite doped with Mn.

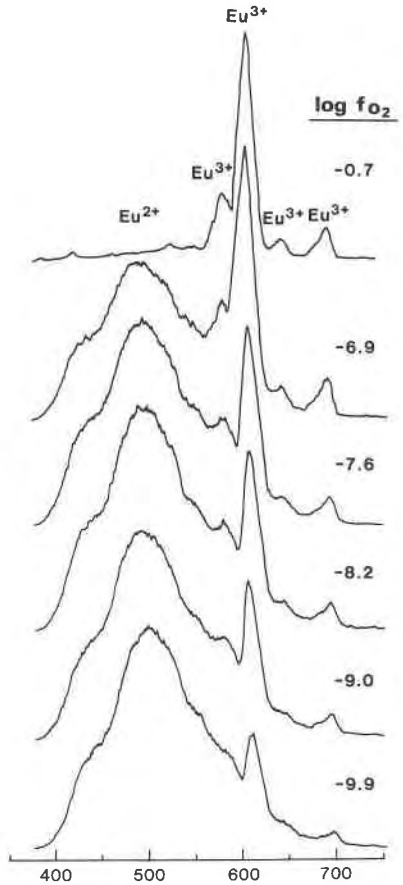

Fig. 5. Cathodoluminescence spectra of glasses doped with Eu and synthesized at a series of oxygen fugacities shown to the right of each spectrum.

in nature, whereas the sample run at log $f_{O_2} = -9.9$ is more reduced for the temperature of synthesis than most conditions expected in nature and is close to the iron-wüstite buffer. The log $f_{O_2} = -6.9$ sample was run at an oxygen fugacity close to the extrapolated value for the quartz-fayalite-magnetite buffer. The four Eu^{3+} peaks of the glasses are at the same wavelength and have the same relative peak height as those in the Llallagua (9) apatite. The broad peak at short wavelengths in the glass samples run at the lower oxygen fugacities is due to Eu^{2+} and is at a higher wavelength ($\lambda = 500$ nm) than the Eu^{2+} peak ($\lambda = 450$ nm) in the Lalllagua and synthetic apatite. Other workers have shown that the Eu^{2+} peak position is sensitive to the structure of the host (Palilla and O'Reilly, 1968). The relative size of the Eu^{3+} and Eu^{2+} peaks in the glasses and calculations using the equation of Drake (1975) suggest that most of the Eu in the Llallagua apatite is in the 3+ state. The relative height of the Eu^{3+} and Eu^{2+} peaks of the Llallagua apatite is closest to the ratio of the peaks for the glass run at log $f_{O_2} = -6.9$. No conclusions can be made, however, as to the relative oxidizing conditions under which the Llallagua apatite crystallized, because we do not know what structural control, if any, there is on the Eu^{3+}/Eu^{2+} ratio in the apatite as compared to the glass. We are suspicious, however, of the assignment of Eu^{2+} to some of the 400–450 nm peaks shown in Figure 3 because of the absence of Eu^{3+} peaks and the very low oxygen fugacities that would apparently be necessary to produce an Eu^{2+} peak such as that in the spectrum of the Durango (1) apatite.

The chondrite-normalized plot of the PIXE-analyzed REEs for the Llallagua apatite is shown in Figure 6 by the circles. The PIXE analyses for all the REEs, except for Eu, were very low and so a Llallagua sample was sent for neutron-activation analysis (NAA) in order to verify that the very strong Eu anomaly was indeed significant. The chondrite-normalized trends in Figure 6 for the PIXE (open circles) and NAA (crosses) analyses are very similar in shape. The neutron-activation analysis of a sample of apatite from the Panasqueira tin deposit in Spain was taken from Knutson et al. (1985) and plotted (solid stars) in Figure 6 for comparison. The very strong positive Eu enrichment for the two apatite samples from separate tin deposits is quite remarkable. Both the PIXE and NAA anal-

yses of the Llallagua apatite show a small positive Sm anomaly that is consistent with Sm, like Eu, being able to sometimes exist in the 2+ oxidation state.

The CL and UV spectra for the Llallagua apatite show mainly Eu^{3+}, and there is no apparent structural reason why apatite should concentrate Eu^{3+} relative to the other REEs. The UV-activated spectrum for the Panasqueira apatite (not shown) shows predominantly Mn^{2+} activation with weaker activation for both Eu^{2+} and Eu^{3+}. The Panasqueria apatite shows quite variable luminescence, both as a mottled pattern and as distinct zonation as reported by Knutson et al. (1985). There are some studies that show a negative Eu anomaly in apatite (Puchelt and Emmermann, 1976; Brunfelt and Roelandts, 1974), and Eby (1975) has suggested that Eu^{2+} may be excluded from apatite because of its size. Thus it seems that the Llallagua apatite, and by inference the Panasqueira apatite, must have crystallized from a reservoir which was strongly enriched in Eu relative to the other REEs. This could have come about by the hydrothermal alteration of plagioclase that had concentrated Eu at some earlier stage. This kind of process is considered in some detail by Graf (1977). Alderton et al. (1980) have shown that the seritization of granite in southwest England produced a negative Eu anomaly and suggested that secondary muscovite can take up REE^{3+} more easily than Eu^{2+}. Thus the resulting hydrothermal fluid may be enriched in Eu relative to the other REEs. There may also be properties of hydrothermal solutions (Flynn and Burnham, 1978) that enhance the transport of Eu^{2+} relative to the trivalent REEs. The difference in field strength of 2+ and 3+ ions may lead to stronger chloride complexes for 2+ ions (e.g., $EuCl^{+}$) and fluoride complexes for 3+ ions. Thus the character of the transporting medium may be as important as the REE composition of the medium in determining the kind of REE distribution in a mineral.

Summary and conclusions

The present study was undertaken in order to determine the relationship between the the color produced by cathodoluminescence and the chemical composition of apatite, in particular the REE distribution. A combination of proton- and electron-microprobe analyses have been used to determine the major- and minor-element content of fourteen apatite samples from various geologic environments. The microprobe analyses of the Durango and Huddersfield apatites compare favorably with published analyses of apatite from the same localities.

The total REE content of the apatites varies from less than 0.2 to more than 15 wt%, and the total number of REE ions is generally proportional to the total number of Na plus Si ions, indicating a charge compensation in the substitution of the REE^{3+} for Ca^{2+}. The amount of Na relative to Si may depend on the alkalinity of the environment of crystallization. Most of the investigated apatites are LREE-enriched with a Ce/Y ratio varying from 30 to less than 0.1. The apatites from alkaline environments tend to show the greatest enrichment in LREEs.

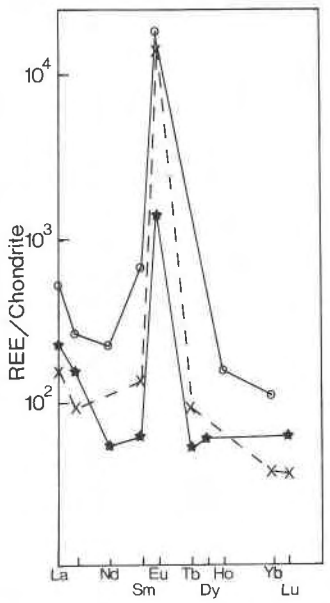

Fig. 6. REEs normalized to the REE content found in a chondritic meteorite for the Llallagua apatite as determined by PIXE (circles) and by neutron activation (crosses) and for the Panasequeira apatite (stars) as reported by Knutson et al. (1985).

The cathodoluminescence spectrum of the apatites was scanned from 400 to 700 nm, and peaks due to Mn^{2+}, Sm^{3+}, Dy^{3+}, Tb^{3+}, Eu^{2+}, and Eu^{3+} were identified. The height of the Sm peaks relative to the Dy peaks was found to be a good indicator of the degree of LREE to HREE enrichment. The resolution of the sharp Sm and Dy peaks in the 600-nm spectral region is diminished in the presence of a broad peak for Mn^{2+}. For example, an apatite from a granite pegmatite (Timmins, Ontario) has a low Mn concentration, but the Mn content is fairly high relative to the REEs, and the CL spectrum shows poor resoltuion of the Sm and Dy peaks because of the broad Mn^{2+} peak. This is contrasted with an apatite from a weathering profile in Australia that contains abundant oxidized manganese oxides (Mn^{4+}), but whose CL spectrum shows good resolution of the Sm and Dy peaks, thus indicating little Mn^{2+} in the apatite structure owing to the oxidizing conditions.

The CL spectrum of an apatite associated with tin mineralization (Llallagua, Bolivia) has a very distinctive CL spectrum with prominent Mn^{2+}, Eu^{2+}, and Eu^{3+} peaks. The chondrite-normalized REE distribution for this sample has a positive Eu anomaly of almost one hundred times the other REEs. The relative height of the Eu^{2+} and Eu^{3+} peaks in the CL and UV-excited spectra were compared to the CL spectra of Eu-doped glasses prepared with various oxygen fugacities at 1400°C. It is concluded that most of the Eu in the Llallagua apatite is Eu^{3+} and that the apatite crystallized from a solution that was strongly enriched in Eu. The apatite structure is thought to concentrate Eu^{3+} relative to Eu^{2+}, and thus no conclusion can be made on the oxidation state of the Eu in the

solution from which the apatite crystallized. Sverjensky (1984) has suggested, however, that hydrothermal solutions at temperatures above 250°C almost certainly contain Eu in the Eu^{2+} state.

The present study has helped to demonstrate the usefulness of cathodoluminescence as a nondestructive geochemical indicator of the environment of crystallization of apatite. This technique provides the petrographer with not only a colorful, but a useful guide to the crystallization history.

Acknowledgments

We are grateful to John S. White, Jr., of the Smithsonian Institution for the Llallagua apatite (sample no. 114175), to T. L. Barry of GTE Sylvania for the Eu^{2+}-, Eu^{3+}-, and Mn^{2+}-doped synthetic apatites, to L. A. Boatner of the Oak Ridge National Laboratory for the REE phosphates, and to C. A. Francis and W. Metropolis of the Harvard Museum for the Panasqueira apatite (sample no. 109117). We gratefully acknowledge the assistance of David Kempson, Larke Zarichny, Ann Mac Donald, and Christopher Peck. Financial support was provided by the Natural Sciences and Engineering Research Council of Canada.

References

Alderton, D.H.M., Pearce, J.A., and Potts, P.J. (1980) Rare earth element mobility during granite alteration: Evidence from southwest England. Earth and Planetary Science Letters, 49, 149–165.

Amli, R. (1975) Mineralogy and rare earth geochemistry of apatite and xenotine from the Gloserheia granite pegmatite, Froland, Southern Norway. American Mineralogist, 60, 607–620.

Bandy, M.C. (1976) Mineralogy of Llallagua, Boliva. Tucson [Arizona] Gem and Mineral Society Special Paper 1.

Brunfelt, A.O., and Roelandts, I. (1974) Determination of rare earth and thorium in apatites by thermal and epithermal neutron-activation analysis. Talanta, 21, 513–521.

Cruft, E.F., Ingamells, C.O., and Muysson, J. (1965) Chemical analysis and the stoichiometry of apatite. Geochimica et Cosmochimica Acta, 29, 581–597.

Drake, M.J. (1975) The oxidation state of europium as an indicator of oxygen fugacity. Geochimica et Cosmochemica Acta, 39, 55–64.

Eby, G.N. (1975) Abundance and distribution of the rare-earth elements and yttrium in the rocks and minerals of the Oka carbonatite complex, Quebec. Geochimica et Cosmochimica Acta, 39, 597–620.

Fleischer, M., and Althschuler, Z.S. (1982) The lanthanides and yttrium in minerals of the apatite group: A review. U.S. Geological Survey Open-File Report 82-783, 1–153.

——— (1986) The lanthanides and yttrium in minerals of the apatite group—An analysis of the available data. Neues Jahrbuch für Mineralogie Monatshefte, 467–480.

Flynn, R.T., and Burnham, C.W. (1978) An experimental determination of rare earth partition coefficients between a chloride containing vapor phase and silicate melts. Geochimica et Cosmochimica Acta, 42, 685–701.

Gold, D.P. (1963) The relationship between the limestones and the alkaline igneous rocks of Oka and St. Hilaire, Quebec. Ph.D thesis, McGill University, Montreal, Quebec.

Graf, J.L., Jr. (1977) Rare earth elements as hydrothermal tracers during the formation of massive sulfide deposits in volcanic rocks. Economic Geology, 72, 527–548.

Grossi Sad, J.H., and Torres, N. (1976) Mineral exploration in the Tapira Complex, Minas Gerais, Brazil. GEOSOL—Geologia e Sondagens Ltda. Belo Horizonte, M.G., Brazil.

Henderson, P. (1980) Rare earth element partition between sphene, apatite and other coexisting minerals of the Kangerdlugssuag intrusion, E. Greenland. Contributions to Mineralogy and Petrology, 72, 81–85.

Henderson, P., Ed (1984) Rare earth element geochemistry. Elsevier Science Publications, B.V.

Huaxin, D. (1980) Cathodoluminescence study of apatite. Geochimica, 4, 368–374.

Jamieson, H.E., and Roeder, P.L. (1984) The distribution of Mg and Fe^{2+} between olivine and spinel at 1300°C. American Mineralogist, 69, 283–291.

Knutson, C., Peacor, D.R., and Kelly, W.C. (1985) Luminescence, color and fission track zoning in apatite crystals of the Panasqueira tin-tungsten deposit, Beira-Baixa, Portugal. American Mineralogist, 70, 829–837.

Kovalenko, V.I., Antipin, V.S., Vladykin, N.V., Smirnova, Ye.V., and Balashov, Yu.A. (1982) Rare-earth distribution coefficients in apatite and behavior in magmatic processes. Geokhimiya, 2, 230–243 (transl. Geochemistry International, 19, 171).

Langurwey, A.A.F. (1977) Detection of trace elements in apatite crystals from Panasqueira, Portugal, by non-destructive optical methods, especially polarspectrography, 6. Scripta Geologica, 42, Leiden.

Lindberg, M.L., and Ingram, B. (1964) Rare-earth silicatian apatite from the Adirondack Mountains, New York. U.S. Geological Survey Professional Paper 501-B, B64–B65.

Ma, Xin-Pei, Palmer, G.R., and MacArthur, J.D. (1987) Element concentrations from overlapping X-ray spectra. Nuclear Instruments and Methods, Physics Research, B22, 49–54.

Marfunin, A.S. (1979) Physics of minerals and inorganic materials. Springer-Verlag, Berlin.

Mariano, A.N. (1978) The application of cathodoluminescence for carbonatite exploration and characterization. Proceedings of the First International Symposium on Carbonatites, Pocos de Caldas, M.G., Brasil, 39–57.

Mariano, A.N., and Ring, P.J. (1975) Europium-activated cathodoluminescence in minerals. Geochimica et Cosmochimica Acta, 39, 649–660.

Mariano, A.N., and Roeder, P.L. (1983) Kerimasi: A neglected carbonatite volcano. Journal of Geology, 91, 449–455.

McKeown, F.A., and Klemic, H. (1956) Rare-earth-bearing apatite, at Mineville, Essex County, New York. U.S. Geological Survey Bulletin, 1046-B, 9–23.

Mitchell, I.V., and Ziegler, J.F. (1977) Ion-induced X-rays. In J.W. Mayer and E. Rimini, Eds., Ion beam handbook for material analysis, p. 311. Academic Press, New York.

Nash, W.P. (1972) Apatite chemistry and phosphorus fugacity in a differentiated igneous intrusion. American Mineralogist, 57, 877–886.

Notholt, A.J.G. (1979) The economic geology and development of igneous phosphate deposits in Europe and the U.S.S.R. Economic Geology, 74, 339–350.

Olson, J.C., Shawe, D.R., Pray, L.C., and Sharp, W.N. (1954) Rare-earth mineral deposits of the Mountain Pass district, San Bernardino County, California. U.S. Geological Survey Professional Paper 261.

Ovcharenko, V.K., and Yurev, L.D. (1971) Luminescence of Ukranian apatites. Doklady Akademiya Nauk Ukr. SSSR, Ser. B, 33, 974–977.

Palilla, F.C., and O'Reilly, B.E. (1968) Alkaline earth halophosphate phosphors activated by divalent europium. Electrochemical Society Journal: Solid State Science, 115, 10, 1076–1081.

Papike, J.J., Jensen, M., Shearer, C.K., Simon, S.B., Walker, R.J., and Laul, J.C. (1984) Apatite as a recorder of pegmatite petrogenesis. Geological Society of America Abstracts with Programs, 16, 617.

Portnov, A.M., and Gorobets, B.S. (1969) Luminescence of apatite from different rock types. Doklady Akademiya Nauk SSSR, 184, 110–113.

Puchelt, H., and Emmermann, R. (1976) Bearing of rare earth patterns of apatite from igneous and metamorphic rocks. Earth and Planetary Science Letters, 31, 279–286.

Roeder, P.L. (1985) Electron-microprobe analysis of minerals for rare-earth elements: Use of calculated peak-overlap corrections. Canadian Mineralogist, 23, 263–271.

Rogers, P.S.Z., Duffy, C.J., Benjamin, T.M., and Maggiore, C.J. (1984) Geochemical applications of nuclear microprobes. Nuclear Instruments and Methods in Physics Research, B3, 671–676.

Shmakin, B.M., and Shiryayeva, V.A. (1968) Distribution of rare earths and some other elements in apatites of muscovite pegmatites, Eastern Siberia. Geokhimiya, 8, 962–969 (transl. Geochemistry International, 796–803).

Sverjensky, D.A. (1984) Europium redox equilibria in aqueous solution. Earth and Planetary Science Letters, 67, 70–78.

Taylor, R.P., and Fryer, B.J. (1982) Rare earth element geochemistry as an aid to interpreting hydrothermal ore deposits. In A.M. Evans, Ed., Metallization associated with acid magnetism, p. 357–365. Wiley, New York.

Trzcienski, W.E., Jr., Perrault, G., and Hebert, P. (1974) A note on apatite from Huddersfield Township, Quebec. Canadian Mineralogist, 59, 289–291.

Watson, E.G., and Green, T.H. (1981) Apatite/liquid partition coefficients for the rare earth elements and strontium. Earth and Planetary Science Letters, 56, 405–421.

Watson, E.B., Harrison, T.M., and Ryerson, F.J. (1985) Diffusion of Sm, Sr, and Pb in fluorapatite. Geochimica et Cosmochimica Acta, 49, 1813–1823.

Young, E.J., Myers, A.T., Munson, E.L., and Conklin, N.M. (1969) Mineralogy and geochemistry of fluorapatite from Cerro de Mercado, Durango, Mexico. U.S. Geological Survey Professional Paper 650-D, D84–D93.

Manuscript received October 14, 1986
Manuscript accepted April 3, 1987

Appendix 1. Sample description of apatites

1. Durango apatite (S-226), Cerro de Mercado mine, Mexico (Young et al., 1969). The famous Durango gem-quality apatites are reported to be generated by hydrothermal reworking of a primary magnetite-apatite igneous body.

2. Huddersfield apatite (S-212), Huddersfield Township, Quebec, Canada (Trzcienski et al., 1974). The apatite occurs in a skarn zone where crystals of apatite, phlogopite, sphene, microcline, and fluorite are in a matrix of pink calcite.

3. Australian supergene apatite (1-G-7) that occurs as botryoidal masses in laterite overlying carbonatite found during a mineral exploration program in Western Australia (collected by A. N. Mariano).

4. Blue river apatite (52-C-6), Bone Creek area of Blue River, British Columbia (collected by A. N. Mariano for the Anschutz Mining Corp., 1982). The apatite occurs as ovoid masses in an apatite beforsite that is predominantly ferruginous dolomite, richterite, and apatite with accessory Ta-rich pyrochlore and zircon. The beforsite is part of the Blue River carbonatite that occurs as concordant sills in the Precambrian Shuswap terrane. The age of the richterite in the carbonatite was found by K-Ar to be 211 ± 10 Ma.

5. Snarum chlorapatite (28-G-1), region between Lallesard and Bamle, southeastern Norway. The chlorapatite is from veins in gabbroic rocks believed to have formed from hydrothermal solutions generated by the intrusion of gabbroic masses into a sedimentary sequence.

6. Pajarito apatite (T-654-0), Otero County, New Mexico (E. E. Foord, S. L. Moore, R. F. Marvin, J. E. Taggart, Jr., unpub., 1983). This apatite is from Pajarito Mountain and is an accessory mineral along with elpidite, zircon, thorite, and allanite in a peralkaline riebeckite syenite. The syenite is part of a series of igneous Proterozoic basement rocks that includes syenites and alkali syenite pegmatites.

7. Timmins (2-E-36), Ontario, Canada. Collected from a granite pegmatite prospect north of Timmins. Apatite occurs with quartz, augite, microcline, sodic plagioclase, calcite, allanite, and trace amounts of thorite, samarskite, hematite, rutile, and fluorite.

8. Kerimasi (3-B-10) volcano, Eastern Rift zone, Tanzania (Mariano and Roeder, 1983). The apatite occurs as euhedral colorless prisms together with magnetite and salite in a melanite-melteigite xenolith in nephelinite and carbonatite agglomerates.

9. Llallagua (8-K-7), Bolivia (Bandy, 1976). The apatite occurs as transparent to translucent pale-pink crystals in the Contacto vein, Siglo XX mine, associated with stannite, cassiterite, jeanbandyite, and crandallite.

10. Mountain Pass (6-E-5), California (Olson et al., 1954). Apatite occurs as euhedral to subhedral colorless prisms that are attached to, or as inclusions in augite, phlogopite, and olivine in shonkinite associated with the Mountain Pass carbonatite.

11. Tapira (29-K-12), Minas Gerais, Brazil (Grossi Sad, and Torres, 1976). The apatite occurs in an early-crystallizing pyroxenite of the Tapira carbonatite complex. The other minerals of the pyroxenite include salite, magnetite, perovskite, and biotite.

12. Khibina (30-D-8) massif, Kirovsk, Kola Peninsula, USSR (J. Gittins, pers. comm., 1985; Notholt, 1979). The Khibina massif consists of an alkaline ring complex with nepheline syenite, foyaites, and carbonatites. A zone of layered ijolite includes high-grade apatite, ijolites, and urtites. The Khibina massif is one of the world's largest sources of phosphate rock.

13. Mineville (1-E-24), New York (McKeown and Klemic, 1956; Lindberg and Ingram, 1964). The apatite occurs with massive magnetite together with gabbro and syenite in Grenville metasedimentary rocks. The mineralogy and texture resemble those of magnetite-apatite rocks (nelsonites) that are often associated with gabbroic anorthosites. The fluoroapatite has been characterized as having anomalous REEs, Y, Th, and U.

14. Oka (5-E-11), Quebec, Canada (Gold, 1963). The apatite occurs as primary colorless prisms associated with calcite, salite, phlogopite, and magnetite in an apatite sovite located near the Britholite zone of the Oka carbonatite.